Vol. 23, No. 2, pp. 216-226 (2023)
Journal of Agricultural Physics
ISSN 0973-032X
http://www.agrophysics.in

Research Article

Assessment of Wheat Yellow Rust Severity Through Hyperspectral Remote Sensing

SOURAMITA CHAKRABORTY, RABI N. SAHOO, DEB K. DAS*, SELVAPRAKASH RAMALINGAM, RAJEEV RANJAN AND J. MUKHERJEE

Division of Agricultural Physics, ICAR- Indian Agricultural Research Institute, New Delhi-110012

ABSTRACT

Remote sensing is increasingly employed in stress management across various agricultural practices, providing real-time analysis for crop stress that visual observation alone cannot achieve. In India, wheat production faces a significant challenge from the yellow rust, caused by the *Puccinia striiformis* f sp. *tritici* fungus. Unfortunately, there is a lack of fundamental information on the spectral signature of wheat yellow rust disease, hindering its real-time detection and management. The current study aims to characterize the spectral reflectance of wheat affected by yellow rust to detect the sensitive spectral range. Ten different wheat genotypes were assessed for disease severity on a scale of 0 to 9, based on the extent of the host organ covered by symptoms or lesions. The results indicate that severely infected plants (score 9) exhibit higher reflectance in the visible region and lower reflectance in the NIR region. The alteration in reflectance for the infected plant, compared to the healthy plant, is more noticeable in the 530-580 nm region in the visible region; 670-740 nm in the red edge region; and 995 nm to 1195 nm in the NIR range showing correlation coefficients exceeding 0.7. An examination of the change in reflectance concerning wavelength (1st derivative) indicates a strong correlation between the VNIR region and disease severity. The red edge position (REP) exhibits the maximum rate of change, referred to as the red edge value (REV), which is closely linked to disease severity levels. The amplitude of the red edge peak diminishes with increasing severity levels, with amplitude values for scores 0 and 9 being 0.009575 and 0.005699, respectively. This research underscores the sensitivity of the VNIR and red edge regions in detecting wheat yellow rust, essential for aerial or satellite-based monitoring of yellow rust-affected wheat cropping regions.

Key words: Wheat, Yellow rust, Spectral signature, Red-edge value

Introduction

Wheat (*Triticum aestivum L.*) holds significant importance as the second most crucial cereal crop in India and contributes significantly to the nation's food and nutritional security. India holds the position of being the second-largest global producer of wheat. To meet the rising food demands sustainably, it is essential to pursue a strategy of integrated pest and disease management. According to Savary *et al.* (2019), biotic constraints account for approximately 21.5% of the current yield losses in wheat. Yellow rust, also known as stripe rust (*Puccinia striiformis f. sp. tritici*), a significant wheat disease particularly in cool and moist climates, holds paramount importance among biotic factors affecting wheat, mainly because of their wide distribution, ability to spread over long distances, and rapid development under favourable environmental conditions. The name "yellow (stripe) rust" is derived from the arrangement of yellow-orange-coloured pustules, extending from one end to another end of the leaves.

*Corresponding author,
Email: dkdas.iari@gmail.com

It starts with the emergence of small, elongated, yellow uredial pustules aligned in rows along the leaf veins. As these pustules mature, they rupture, releasing a yellow-orange mass of urediospores. After the plants are infected and reach maturity or experience stress, their tissues turn brown and dry, giving the plants a withered and scorched appearance. Continuous monitoring, precise quantification of disease severity, and effective control methods are imperative in the current situation. Traditionally, assessing the extent of diseases and pest damage in a large plant population relied on visually observing symptomatic plants, a process known for its time and labour intensiveness. Moreover, visual assessments struggle to accurately and swiftly gauge disease severity when plants react to abiotic stress situations like drought, extreme temperatures, edaphic conditions, and high winds. The challenges arise from the difficulty in visually quantifying these responses with acceptable levels of accuracy and speed. However, plant responses to infection often influence the quantity and quality of electromagnetic radiation reflected from the plant canopy (Nutter *et al.*, 2002). This suggests that employing remote sensing techniques could offer a readily available means of recording disease severity, providing a more objective assessment compared to visual evaluations conducted by raters (Coops *et al.*, 2003; Apan *et al.*, 2004; Sankaran *et al.*, 2012).

Especially reflectance instituted to be capable of detecting changes in the biophysical properties of plants and canopies associated with pathogens (Moran *et al.*, 1997; Moshou *et al.*, 2005; Jensen, 2007; Ranjan *et al.*, 2012; Sahoo *et al.*, 2015). In addition, remote sensing may provide a greater means to objectively quantify disease stress than visual assessment methods, and it can be used to repeatedly collect sample measurements non-destructively and non-invasively (Nilsson, 1995; Moran *et al.*, 1997). Distinctive alterations in the reflectance spectrum have been noted in various plant diseases, such as yellow rust in wheat (Bravo *et al.*, 2003), powdery mildew in wheat (Graeff *et al.*, 2006), late blight in tomatoes (Wang *et al.*, 2008), and yellow mosaic virus in soybeans (Gazala *et al.*, 2013). While commonly used broadband techniques have proven effective in distinguishing between healthy and diseased plants (Sharp *et al.*, 1985; Lorenzen and Jensen, 1989; Nicolas, 2004), the differentiation between healthy plants and those exhibiting mild symptoms is not always precise. Nonetheless, the continuous measurement of reflectance (hyperspectral remote sensing), utilizing a series of narrow wavelength bands, furnishes relevant information for accurately discerning diseases and other stresses affecting plants. Detecting specific spectral reflectance associated with wheat yellow rust infection through remote sensing is crucial for large-scale assessment and monitoring of yellow rust disease in wheat fields, particularly for strategic crop management decisions and predicting yield losses. However, to date, there has been no investigation into characterizing the reflectance spectra of wheat to evaluate yellow rust disease in India. The primary aim of this current study was to analyze the reflectance spectra linked to yellow rust infection in wheat, to utilize remote sensing data for disease detection across extensive areas.

Materials and Methods

Experimental area

A field experiment was conducted, in the New Area farm of ICAR-Indian Agricultural Research Institute, New Delhi (28°4′ N latitude, 77°09′ E longitude and at an altitude of 228.16 m above msl) with wheat as a test crop in the *rabi* season of the year 2022-23.10 different wheat genotypes were sown among which there was a different level of yellow rust infestation due to their different resistance against the yellow rust pathogen (Table 1).

Table 1. Disease rating scale of respective wheat genotypes in IARI farm

Genotype name	Disease Severity score
HD 3406	0
HD 3086	1
DL 22 -16	2
HD 3454	3
HD 3407	4
DL 22-4	5
HD 3293	6
HD 3059	7
HD 2932	8
HD 2967	9

Spectral observations of the wheat canopy at two different dates were taken during the peak infestation period at the anthesis and grain filling stage respectively. The climate in New Delhi can be broadly categorized as subtropical and semiarid, characterized by hot and dry summers as well as cold winters. During the infection period, the mean temperature fluctuated from 8.5 to 13.8. Maximum relative humidity during the disease infection period was varying from 98% to 65%. The total rainfall received during the growing season was 136.1 mm.

Measurement of spectral reflectance of wheat under different gradient of yellow rust severity

The assessment of yellow rust severity was conducted once suitable stress conditions were established, and observations were recorded for various severity levels. The disease severity ratings ranged from 0 to 9, by the scale provided by McNeal *et al.* (1971) (Table 2).

The canopy reflectance of the wheat at IARI field was assessed using a handheld ASD FieldSpec4 Std-Res Spectroradiometer (Analytical Spectral Devices Inc., Boulder, CO, USA). The spectral resolution is 3 nm at 700 nm, 8 nm at 1400-2100 nm with sampling intervals (bandwidths) of 1.4 nm at 350-1000 nm and 1.1 nm at 1001-2500 nm. The captured data was then resampled to 1 nm bandwidth for all the measurements. This was carried out to measure disease severity across 10 levels on a scale of 0 to 9, in 10 distinct wheat genotypes. The measurements were conducted on a clear and sunny day between 11:00 am and 1:00 pm. The spectroradiometer, affixed with a 25° field of view (FOV), was positioned at a distance of 1 meter from the top of the canopy in a nadir orientation. Before capturing the spectral reflectance, the instrument's optimization was ensured using a white reference panel known as spectralon (Labsphere, Inc. based in Sutton, NH, USA) which shows 100% reflectance. Reference reflectance was initially measured to calibrate the spectroradiometer, followed by the actual canopy reflectance measurements. Each spectral measurement represented an average derived from 30 spectral scans of the sample. The optimization process was reiterated whenever there was a shift in solar irradiance during spectral observations. The spectral range for these measurements spanned from 350 to 2500 nm.

Pre-processing of spectroscopic data

The primary objective of pre-processing is to mitigate the impact of random noise and amplify the signal-to-noise ratio. One of the most frequently employed filters in the analysis of spectral data is the Savitzky-Golay filter. This filter employs a moving polynomial fit of varying orders, and its filter size is determined by the formula (2n+1) points, where 'n' signifies half the width of the smoothing window. The data points situated between these two 'n' values are interpolated using the polynomial fit technique (Savitzky and Golay, 1964).

Correlation analysis of spectral reflectance and disease severity

The correlation analysis between spectral reflectance and disease severity was performed to identify the different spectral regions sensitive to

Table 2. Disease rating scale of respective wheat genotypes in IARI farm

Rating	Description
Score 0	No visible disease symptoms
Score 1	Minor chlorotic and necrotic flecks
Score2	Chlorotic and necrotic flecks without sporulation
Score 3	Chlorotic and necrotic areas with very limited sporulation
Score 4	Chlorotic and necrotic areas with limited sporulation
Score 5	Chlorotic and necrotic areas with moderate sporulation
Score 6	Chlorotic and necrotic areas with moderate to high sporulation
Score 7	Abundant sporulation with moderate chlorosis
Score 8	Abundant sporulation without chlorosis
Score 9	Abundant and dense sporulation without chlorosis and necrosis

yellow rust disease. In this study, the correlation value 0.6 was considered as a threshold to identify the sensitive spectral regions

Development of spectral derivatives and red edge analysis

The initial derivative of the mean reflectance was computed, and an appropriate order of polynomial fitting was executed using the least squares method (Savitzky and Golay, 1964). Investigation into red edge shifts and the configuration of the red peak in the first derivative curve was conducted across various degrees of disease severity. For each infection level, the wavelength (kre) and amplitude (drre) of the red peak were determined through a linear interpolation technique, achieved by fitting a second-order polynomial equation to the red infrared slope (Guyot *et al.,* 1988). The spectral characterization under different disease scores involved assessing the red edge parameters, specifically λre (the wavelength of the red edge peak), drre (the amplitude of the red edge peak in the first derivative reflectance curve), and Σ(dr 670–780) (the sum of the first derivative reflectance amplitudes between 670 and 780 nm).

Results and Discussion

Scoring of yellow rust disease infection

The disease severity levels were estimated by evaluating the percentage of host tissue covered by the chlorotic and necrotic lesions of the disease and the degree of sporulation. The extent of wheat yellow rust severity was graded from 0-9. The severity level 0 depicts that the plant is healthy having no symptoms at all and the disease severity level 9 depicts that the plant is most severely affected by the pathogen. The disease severity levels; in-between show various levels of infestation and severity level gradually increases from 0 to level 9. Wheat genotypes, HD 2967 and HD 3406 grown under irrigated conditions were assigned as level 9 and level 0 respectively. The details of other varieties and their corresponding severity levels are shown in Table 1.

Response to leaf reflectance pattern with severity levels of the wheat plant

This investigation revealed a distinct spectral response that varied with the degree of disease infestation. The graphical representation in Fig. 1 illustrates the evolving patterns in leaf reflectance across different levels of disease infestation. As the severity of the disease increased, there was a noticeable rise in reflectance in the visible region, particularly in the red region, where the reflectance was higher in severely affected plants compared to healthy ones. The spectral reflectance in this specific region was primarily affected by the content of leaf pigments. In plants infected with yellow rust, the pathogen substantially damaged the plant chlorophyll.

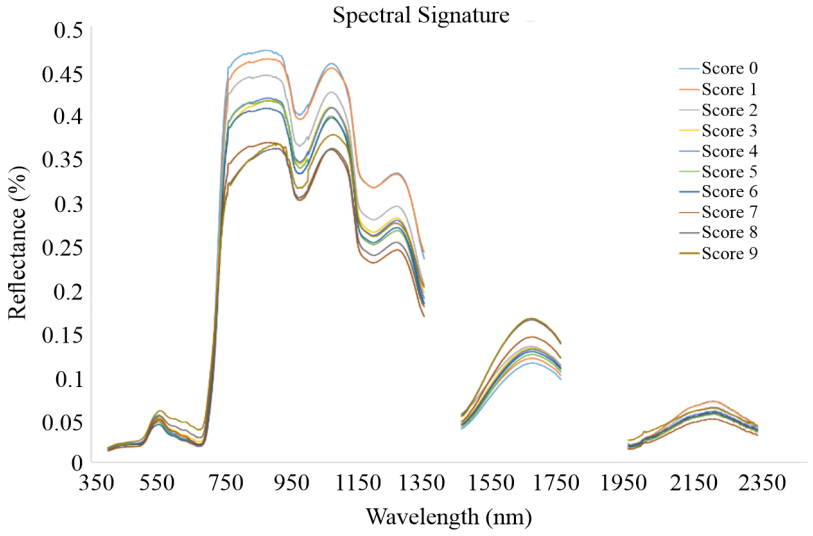

Fig. 1. Spectral reflectance of yellow rust infected wheat canopy under various severity levels at IARI farm

In the near-infrared (NIR) region, the reflectance of a healthy plant surpasses that of an infected one, and as the severity of the disease increases, the reflectance in the NIR region gradually diminishes (Fig. 1). This reduction in reflectance is associated with the severe infection by the pathogen, prompting the plant to generate reactive oxygen species such as hydrogen peroxide and facilitating cellulose deposition at the infection site (Thordal-Christensen *et al.*, 1997; Nishimura *et al.*, 2003). These processes are key contributors to the formation of necrotic lesions, resulting in cell damage and eventual plant death. Similar observations were reported by Das *et al.* (2013) for soybean crops infected with yellow mosaic virus, indicating a decrease in reflectance in the NIR region. In the shortwave infrared (SWIR) region, the severely affected plant exhibits higher reflectance compared to the plant infected with the disease, potentially attributed to lower leaf water content in yellow rust-infected plants.

The disparity in reflectance between wheat plants at various severity levels (score 1 to 9) and that of a healthy plant was calculated and depicted across the spectral range of 350 to 2500 nm (see Fig. 2). The spectral regions where the contrast is notably pronounced include the yellow band (560 to 590 nm), red band around 680 to 690nm and the near-infrared (NIR) range, specifically spanning from 830 to 1300nm. As the severity increases, there is a more positive difference in the red band and a more negative difference in the NIR range. Additionally, a positive difference in reflectance was observed in the shortwave infrared region. The absorption in the visible range (400-700 nm) is predominantly characterized by electron transitions in chlorophyll and other plant pigments.

In the near-infrared (NIR) and shortwave infrared (SWIR) spectral ranges, the spectral reflectance is significantly impacted by the bending and stretching of the O-H bond in water and other molecules, resulting in distinctive absorption peaks occurring at wavelengths of 970 nm, 1145 nm, 1400 nm, and 1940 nm (Curran, 1989). The reflectance in the near-infrared region (700-1100 nm) is primarily influenced by the internal leaf structure. Within the NIR spectral range, the internal mesophyll structure undergoes multiple reflections due to differences in the refractive index of the cell wall and the internal air cavity, namely the vacuole. As a result, plants typically exhibit higher reflectance in this region. In the shortwave infrared region (1100-2500 nm), reflectance is influenced by the composition of leaf chemicals and water content (Jacquemoud and Ustin, 2001).

Relationship between disease score and reflectance pattern

The spectral reflectance at each wavelength exhibited varying levels of correlation with the disease severity scores, ranging from 0 to 9, across

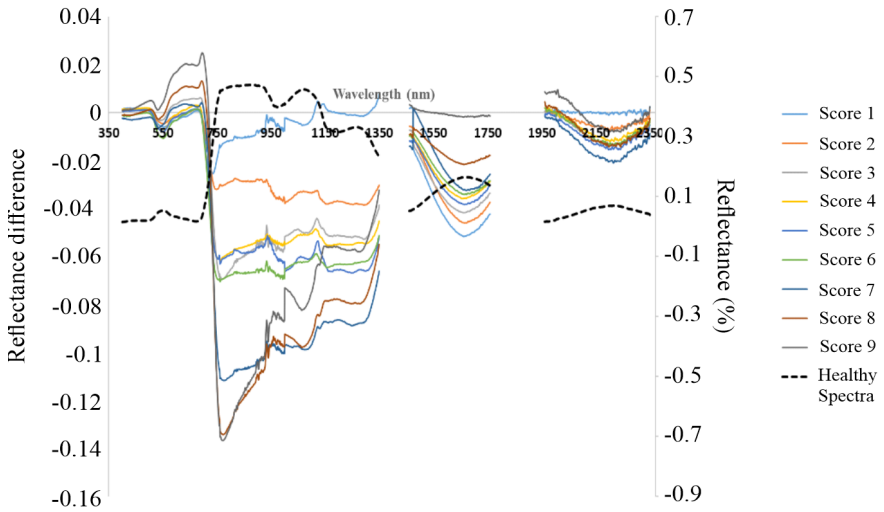

Fig. 2. Spectral reflectance difference of infected wheat plant with different severity levels with reference to healthy wheat crop

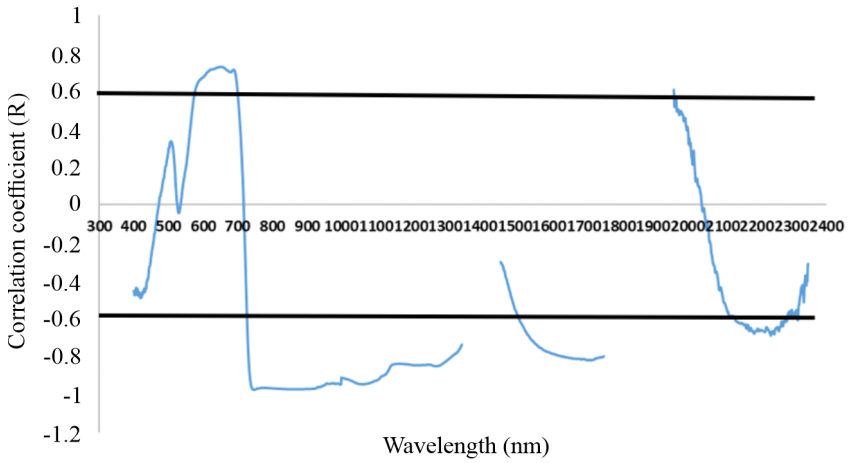

Fig. 3. Correlation coefficient (r) between reflectance spectra of wheat plants at different wavelength with different severity levels of yellow rust infestation in field experiment

the entire spectral range of 350 to 2500nm (depicted in Fig. 3). The correlation analysis highlighted certain spectral ranges that displayed a strong relationship with the score values. By considering a correlation value of 0.6 or higher as the threshold, specific wavelength regions that were connected to disease scores emerged, notably at 580nm, 695nm, and 754nm in the visible region of the spectra. The entire region of 750 nm to 1340 nm (Near-infrared region) as well as in the SWIR-1 region from 1560 to 1756 nm, and within the span of SWIR-2 region from 2134 nm to 2320 nm showed a significant negative correlation with disease score for all the wheat genotypes cultivated in field conditions.

The yellow rust pathogen is an obligate biotrophic parasite. The cytoplasm of a urediniospore travels into the developing germ tube as it grows over the leaf surface (Kang *et al.*, 2002) perpendicular to the long axis of epidermal cells before it reaches stoma (Wang *et al.*, 2009). When hypha comes in contact with the mesophyll cell, a haustorial mother cell having two to six nuclei forms and most of the cytoplasm transfers into the haustorial mother cell (Kang *et al.*, 2002). Haustorial mother cell has a thick multi-layered wall that attaches firmly to the host cell wall and from there a balloon-shaped feeding structure, called Haustorium is generated. The primary infection hypha will give rise to many branched hyphae that expand between host mesophyll cells and produce multiple haustorial mother cells and haustoria, leading to a branching network of fungal mycelium establishing inter- and intracellularly within the host tissue by slowly destroying the internal mesophyll cell structure.

As a result of the intense infection caused by the pathogen, the plant initiates the generation of reactive oxygen species such as hydrogen peroxide and the deposition of callose at the infection site (Thordal-Christensen *et al.*, 1997; Nishimura *et al.*, 2003). These processes are the primary factors contributing to the development of necrotic lesions, ultimately leading to cell damage and the eventual demise of the plant. Callose, a plant polysaccharide produced as a temporary cell wall in response to disease stress, plays a crucial role in inducing significant changes in spectral reflectance values in the near-infrared (NIR) ranges. The pathogen profoundly impacts the mesophyll cells, nearly causing the plant's demise. Consequently, at disease severity level 9, there is minimal distinction between the spectra of the soil and the plant, as the plant is on the verge of death.

Response and relationship of 1st derivative of canopy reflectance to disease severity levels

1st derivative of spectral responses was calculated to identify the sensitive band or the sensitive range of the whole spectra responsible for yellow rust severity assessment (Fig. 4). 1st derivative canopy reflectance was correlated with the measured disease score levels (Fig. 5). Threshold limit for both positive and negative correlation

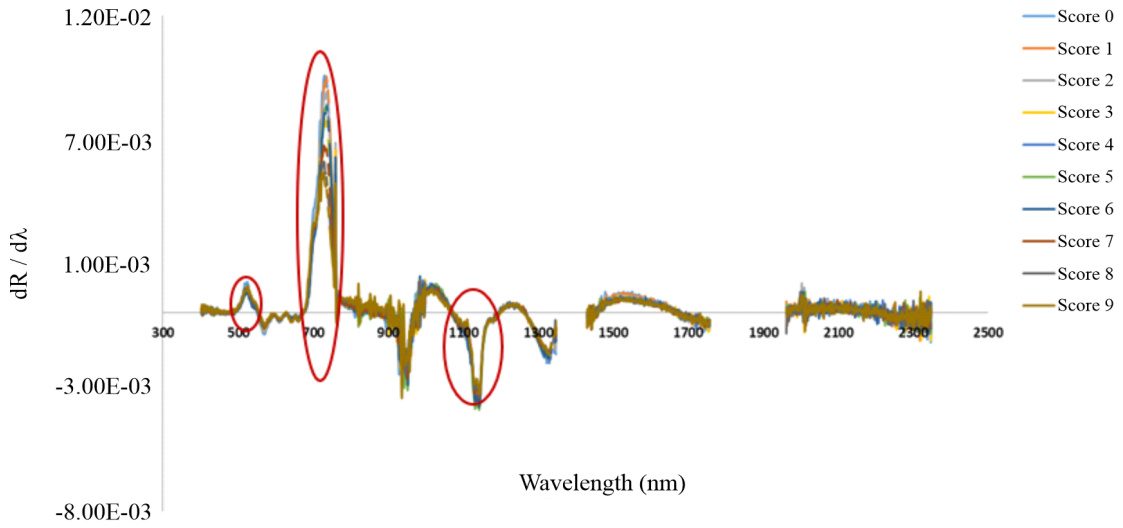

Fig. 4. Characterization of differential infestation levels of yellow rust by Spectral Derivatives of reflectance of wheat plants at various yellow rust severity at the field experiment

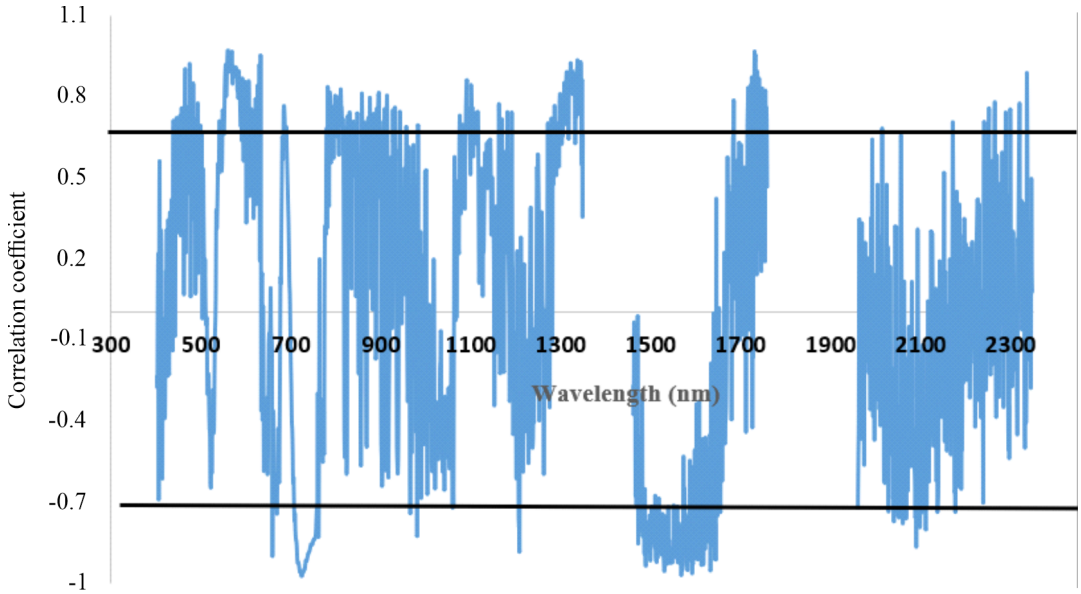

Fig. 5. Sensitive spectral ranges for disease severity through correlation analysis of 1st derivative of spectral reflectance with disease score values

coefficient was considered as 0.7. Very distinguished observations were found in some specific bandwidths. From the 1st derivative reflectance spectra, the visible and NIR region of the whole spectra were found to be responsive to yellow rust. Specifically, 530-580 nm region in the visible region; 670-740 nm in the transition zone of the visible-NIR region; and 995 nm to 1195 nm in the NIR range showed distinct responses among all the severity levels. Correlation of 1st derivative reflectance was found better in visible, NIR and SWIR-1 regions of electromagnetic spectra (Fig. 5). Higher correlation was obtained in the region of 460-512, 532-653 and 680-760 nm. 460-512 and 680-760 nm regions were positively correlated whereas 532-653 nm region was negatively correlated. A high correlation was also observed at a few spectral values in the ranges of 995-1195 nm and 1500-1740 nm of SWIR regions.

Utilizing mathematical transformations on the reflectance data and deriving the first derivative enabled the detection of distinct spectral ranges responsive to different degrees of severity in wheat yellow rust disease. By assessing the red edge region of the spectral reflectance (680-760 nm) based on first derivative values, a notable correlation was observed between the red edge value (REV) and disease scores. Confirming the sensitivity of the red edge region to disease severity levels, correlations between the first derivative of spectral reflectance and disease scores were evident. The pathogen responsible for wheat yellow rust disease causes damage to the cell structure, leading to the drying of the plant and the formation of necrotic spots. This damage to the plant's chlorophyll content has a discernible impact on the red edge value. Furthermore, the correlation of disease score values in the NIR ranges (995-1195 nm) and SWIR ranges (1500-1740 nm) is influenced by the combined effects of cell structure damage and the loss of cell water. The collective impact of diminished chlorophyll content and cellular structure damage designates the VNIR region as the most sensitive for disease detection.

Influence of disease severity levels on red edge value

The red edge region is typically defined as the spectral range spanning from 680 to 760nm. Within this red-edge region, there is a highly noticeable and distinctive change in reflectance as wavelengths vary, which is valuable for detecting crop stress. When examining a plant with varying stress levels, two common observations are made in this spectral range. One is the occurrence of an inflection point where the rate of reflectance change transits from positive to negative, this inflection point is referred to as the red edge position (REP). Under the influence of stress, REP moves towards shorter wavelengths, known as a blue shift. Conversely, during the plant's recovery from stress and return to a healthy state, REP shifts towards longer wavelengths, referred to as a redshift. The maximum rate of change occurring at the red edge position is termed as the red edge value (REV), which exhibits a significant connection with stress levels. REV represents the highest point of the first derivative of reflectance. The distinct difference among all the stress levels was depicted in 730 nm region, known as the red edge value. However, in this case, a dip in the curve is observed at the wavelength of 721 nm (Fig. 6). The peak of this dip progressively decreases as the severity of the disease increases, as illustrated in Fig. 6. This is consistent with findings by Mahlein *et al.* (2010) who found similar red edge reflection patterns studying sugar beet leaves infected with fungal diseases such as *C. beticola* and *U. betae*. When a plant is significantly impacted by the condition, the curve's incline is less pronounced compared to that of a

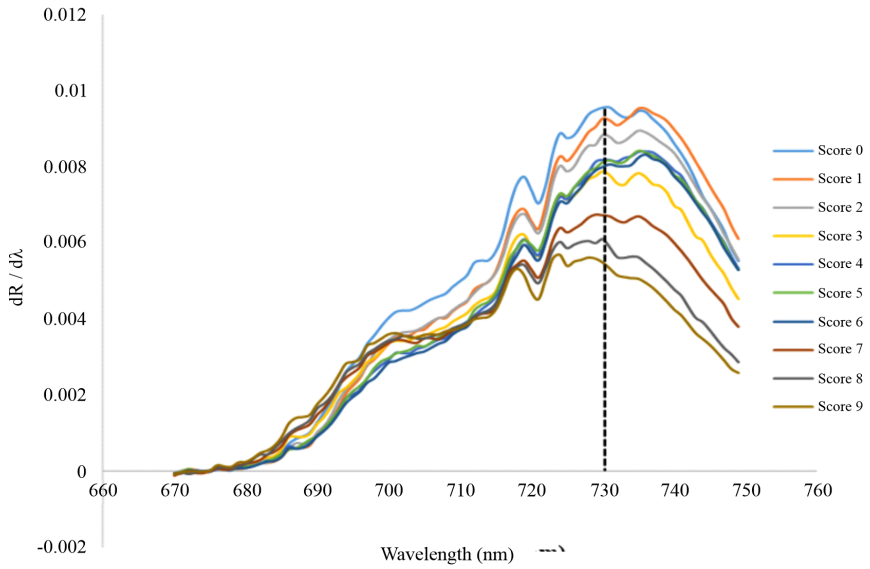

Fig. 6. Red edge curve of yellow rust infected wheat canopy in field condition

Table 3. Characteristics of red edge amplitude with various disease score levels

Disease score	Amplitude of red edge peak	Sum of 1st derivative reflectance amplitude between 680-760 nm
0	0.009575	0.443339
1	0.009547	0.400135
2	0.00896	0.351815
3	0.008434	0.331267
4	0.008409	0.310585
5	0.008337	0.293136
6	0.00789	0.259050
7	0.00675	0.233420
8	0.006101	0.199413
9	0.005699	0.167853

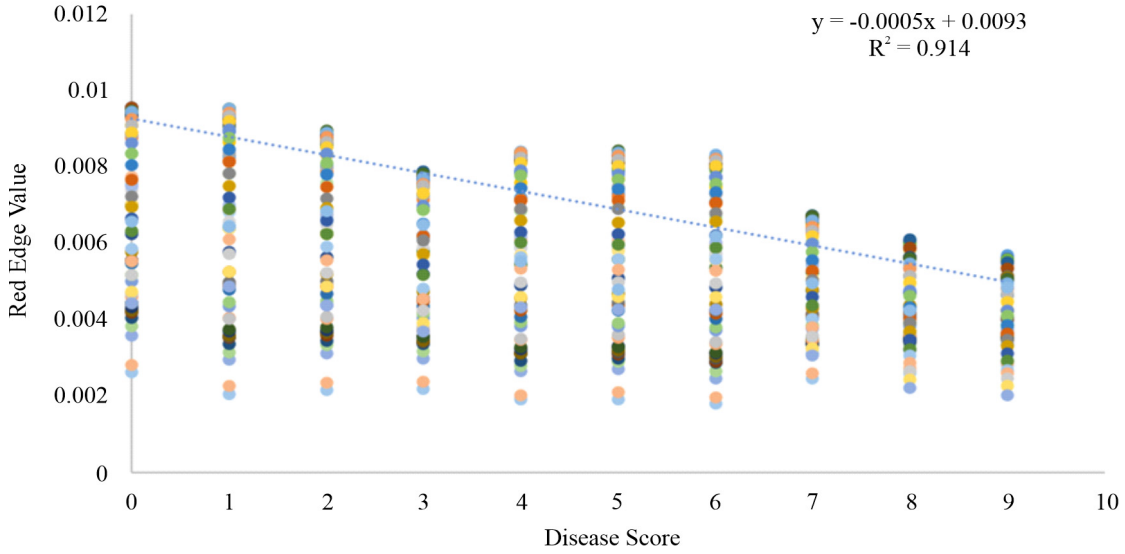

Fig. 7. Relationship between measured disease score values with the red edge values

healthy plant. The data in Table 3 indicates a gradual reduction in both the peak magnitude and the cumulative value of the initial derivative of reflectance within the range of 680-760 nm as the disease severity escalates. Amplitude of scores 0 and 9 was 0.009575 and 0.005699, respectively (Table 3). Fahrentrapp *et al.*(2019) reported similar findings about red edge amplitude for gray mold leaf infections. A robust association between the severity of the disease and REV was identified, demonstrating a substantial coefficient of determination (R^2) of 0.91 illustrated in Fig 7.

Conclusions

The study highlights the potential of hyperspectral remote sensing not only in characterizing wheat crops infected with yellow rust disease but also in identifying specific bands that are sensitive for assessing the severity of the infection. Noticeable differences in spectral reflectance were observed across various disease severity levels, particularly in the visible and near-infrared (VNIR) range. The application of spectral transformations, specifically the first derivative (red edge) pinpointed the most sensitive spectral ranges as 460 to 760 nm in the VNIR range and 1500 to 1740 nm in the shortwave infrared region for assessing the yellow rust severity levels. The utilization of a predictive model for yellow rust disease, incorporating the red edge value (REV) with R^2 values of 0.91, surpassing the 0.6 threshold, indicates significant potential for upscaling in field-scale applications. This could be achieved using recently developed multispectral cameras equipped with a red edge band on airborne platforms, such as unmanned aerial vehicles.

References

Apan, A., Held, A., Phinn, S. and Marley, J. 2004. Detecting sugarcane 'orange rust' disease using

EO-1 Hyperion hyperspectral imagery. *International Journal of Remote Sensing* **25**: 489-498.

Bravo, C., Moshou, D., West, J., McCartney, A. and Ramon, H. 2003. Early disease detection in wheat fields using spectral reflectance. *Biosystems Engineering* **84**(2): 137-145.

Coops, N., Stanford, M., Old, K., Dudzinski, M., Culvenor, D. and Stone, C. 2003. Assessment of Dothistroma needle blight of Pinus radiata using airborne hyperspectral imagery. *Phytopathology* **93**(12): 1524-1532.

Curran, P.J. 1989. Remote sensing of foliar chemistry. *Remote Sensing of Environment* **30**(3): 271-278.

Das, D.K., Pradhan, S., Sehgal, V.K., Sahoo, R.N., Gupta, V.K. and Singh, R. 2013. Spectral reflectance characteristics of healthy and yellow mosaic virus-infected soybean (*Glycine max* L.) leaves in a semiarid environment. *Journal of Agrometeorology* **15**(1): 36-38.

Fahrentrapp, J., Ria, F., Geilhausen, M. and Panassiti, B. 2019. Detection of gray mold leaf infections prior to visual symptom appearance using a five-band multispectral sensor. *Frontiers in Plant Science* **10**: 628-635

Gazala, I.F., Sahoo, R.N., Pandey, R., Mandal, B., Gupta, V.K., Singh, R. and Sinha, P. 2013. Spectral reflectance pattern in soybean for assessing yellow mosaic disease. *Indian Journal of Virology* **24**(2): 242-249.

Graeff, S., Link, J. and Claupein, W. 2006. Identification of powdery mildew (*Erysiphe graminis* sp. *tritici*) and takeall disease (*Gaeumannomyces graminis* sp. *tritici*) in wheat (*Triticum aestivum* L.) by means of leaf reflectance measurements. *Open Life Science* **1**(2): 275-288.

Guyot, G., Baret, F. and Major, D.J. 1988. High spectral resolution: determination of spectral shifts between the red and the near infrared. *International Society for Photogrammetry and Remote Sensing* **11**: 750-760.

Jacquemoud, S. and Ustin, S.L. 2001. January. Leaf optical properties: A state of the art. In *8th International Symposium of Physical Measurements & Signatures in Remote Sensing* (pp. 223-332). CNES Aussois France.

Jensen, J.R. 2007. In *Remote sensing of the environment: an earth resources perspective. 2nd ed*. New Jersey: Pearson Education Inc. pp 12-56.

Kang, Z., Huang, L. and Buchenauer, H. 2002. Ultrastructural changes and localization of lignin and callose in compatible and incompatible interactions between wheat and *Puccinia striiformis*. *Journal of Plant Diseases and Protection* **109**: 25-37.

Lorenzen, B. and Jensen, A. 1989. Change in leaf spectral properties induces in barley by cereal powdery mildew. *Remote Sensing of Environment* **27**: 201-209.

Mahlein, A.K., Steiner, U., Dehne, H.W. and Oerke, E.C. 2010. Spectral signatures of sugar beet leaves for the detection and differentiation of diseases. *Precision Agriculture* **11**: 413-431.

McNeal, F.H., Konzak, C.F., Smith, E.P., Tate, W.S. and Russell, T.S. 1971. In *A uniform system for recording and processing cereal research data* (No. REP-10904. CIMMYT).

Moran, S., Inoues, Y. and Barnes, E.M. 1997. Opportunities and limitations for image-based remote sensing in precision farming. *Remote Sensing of Environment* **61**: 319-346.

Moshou, D., Bravo, C., Oberti, R., West, J., Bodria, L., McCartney, A. and Ramon, H. 2005. Plant disease detection based on data fusion of hyper-spectral and multi-spectral fluorescence imaging using Kohonen maps. *Real-Time Imaging* **11**(2): 75-83.

Nicolas, H. 2004. Using remote sensing to determine of the date of a fungicide application on winter wheat. *Crop Protection* **23**(9): 853-863.

Nilsson, H. 1995. Remote sensing and image analysis in plant pathology. *Annual Review Phytopathology* **33**(1): 489-528.

Nishimura, M.T., Stein, M., Hou, B.H., Vogel, J.P., Edwards, H. and Somerville, S.C. 2003. Loss of a callose synthase results in salicylic acid-dependent disease resistance. *Science* **301**(5635): 969-972.

Nutter Jr, F.W., Guan, J., Gotlieb, A.R., Rhodes, L.H., Grau, C.R. and Sulc, R.M. 2002. Quantifying alfalfa yield losses caused by foliar diseases in Iowa, Ohio, Wisconsin, and Vermont. *Plant Disease* **86**(3): 269-277.

Ranjan, R., Chopra, U.K., Sahoo, R.N., Singh, A.K. and Pradhan, S. 2012. Assessment of plant nitrogen stress in wheat (*Triticum aestivum* L.) through hyperspectral indices. *International Journal of Remote Sensing* **33**(20): 6342-6360.

Sahoo, R.N., Ray, S.S. and Manjunath, K.R. 2015. Hyperspectral remote sensing of agriculture. *Current Science* 848-859.

Sankaran, S., Ehsani, R., Inch, S.A. and Ploetz, R.C. 2012. Evaluation of visible-near infrared reflectance spectra of avocado leaves as a non-destructive sensing tool for detection of laurel wilt. *Plant Disease* **96**(11): 1683-1689.

Savary, S., Willocquet, L., Pethybridge, S.J., Esker, P., Mc Roberts, N. and Nelson, A. 2019. The global burden of pathogens and pests on major food crops. *Nature Ecology and Evolution* **3**: 430-439.

Savitzky, A. and Golay, M.J. 1964. Smoothing and differentiation of data by simplified least squares procedures. *Analytical Chemistry* **36**(8): 1627-1639.

Sharp, E.L., Perry, C.R., Scharen, A.L., Boatwright, G.O., Sands, D.C., Lautenschlager, L.F., Yahyaoui, C.M. and Ravet, F.W. 1985. Monitoring cereal rust development with a spectral radiometer. *Phytopathology* **75**(8): 936-939.

Thordal Christensen, H., Zhang, Z., Wei, Y. and Collinge, D.B. 1997. Subcellular localization of H2 O2 in plants. H2 O2 accumulation in papillae and hypersensitive response during the barley-powdery mildew interaction. *The Plant Journal* **11**(6): 1187-1194.

Wang, X., Tang, C., Zhang, G., Li, Y., Wang, C., Liu, B., Qu, Z., Zhao, J., Han, Q., Huang, L. and Chen, X. and Kang, Z. (2009). cDNA-AFLP analysis reveals differential gene expression in compatible interaction of wheat challenged with *Puccinia striiformis* f. sp. *tritici*. *BMC Genomics* **10**(1): 1-12.

Wang, X., Zhang, M., Zhu, J. and Geng, S. (2008). Spectral prediction of Phytophthora infestans infection on tomatoes using artificial neural network (ANN). *International Journal of Remote Sensing* **29**(6): 1693-1706.

Received: 14 May 2023; Accepted: 5 August 2023